Korean J. Chem. Eng., 36(6), 837-842 (2019)
DOI: 10.1007/s11814-019-0272-4

pISSN: 0256-1115
eISSN: 1975-7220

Vortex generation by viscoelastic sheath flow in flow-focusing microchannel

Dong Young Kim* and Ju Min Kim*,,†**

*Department of Energy Systems Research, Ajou University, Suwon 16499, Korea
**Department of Chemical Engineering, Ajou University, Suwon 16499, Korea
(*Received 17 March 2019 • accepted 8 April 2019*)

Abstract−Microfluidics-based technologies have attracted much attention since the fluid flow can be controlled precisely and only small sample volumes are required. Viscoelastic non-Newtonian fluids such as polymer solution and biofluids are frequently used in microfluidic analyses, and it is essential to understand the small-scale flow dynamics of such viscoelastic fluids. In this work, we report on vortex generation at the junction region of a flow-focusing microchannel, where a central flow stream of a Newtonian fluid meets two sheath flows of a non-Newtonian poly (ethylene oxide) aqueous solution. We elucidated the vortex-generation mechanism by the backward-flow component induced by the first normal stress difference in the viscoelastic sheath fluid. We systematically investigated the effects of polymer concentration, total flow rate, and total to central-stream flow-rate ratio, on the vortex generation. In addition, we demonstrated that this phenomenon can be engineered to enhance the mixing in the flow-focusing microchannel. We expect this work to be helpful for the understanding of viscoelastic flow dynamics in microscale flows and also for the development of microfluidic mixers.

Keywords: Viscoelastic Fluid, Flow-focusing Microchannel, Normal Stress Difference, Vortex Generation

INTRODUCTION

Microfluidics-based approaches have recently been applied to a wide range of applications, such as biological analysis and fine chemical synthesis [1,2]. Material synthesis in microchannels, in particular, has attracted much attention, as the flow can be controlled accurately for continuous synthesis, and the whole process from material synthesis to analysis can be integrated into a single chip [2]. For example, the production of highly uniform non-spherical particles was demonstrated utilizing microfluidic methods [3]. However, flows in microfluidic channels are typically laminar, because of the low Reynolds number (Re) conditions due to the small-length scales of the microchannel [4]. Therefore, mixing remains a challenging issue in many microreactor applications [5]. Highly complicated channel structures have been devised to enhance the mixing of fluid streams in a three-dimensional serpentine channel [6] or in herringbone-type microchannels [7].

The generation of turbulent flows, even at very low Re conditions, was demonstrated when viscoelastic fluids such as polymer solutions flowed along curved streamlines [8-10]; this is now termed "elastic turbulence" [9]. Flow instability in viscoelastic fluids was observed in various flow situations such as micro-contraction flows [11], which were recently used for microfluidic mixing [12]. The microfluidic mixer based on the viscoelastic instability can be implemented using simple single-layer channels, which is more beneficial than the conventional schemes that require complicated structures for Newtonian fluids [5]. In this work, we propose a novel microfluidic mixing scheme that utilizes the vortex generated in a flow-focusing geometry, when viscoelastic fluids are used for sheath flows.

Flow-focusing geometry is typically composed of one central fluid stream and two sheath flows, as shown in Fig. 1. Microfluidic flow-focusing geometry has been widely used for mixing by diffusion [5], where the central stream is tuned thinly with the sheath flows to enhance the mixing by decreasing the diffusion length [4]. Flow dynamics in flow-focusing geometry has been extensively studied owing to its importance in such practical applications [4,13,14]. The flow patterns demonstrate the extensional flow fields arising from convergent flow (Fig. 1(b)), when both central and sheath flows are Newtonian. On the other hand, it is found that a pair of vortices are generated at the junction of the central and sheath fluid streams when both the central and sheath flows are Newtonian and the ratio of the average velocity in the central stream to that in the sheath stream (VR) is significantly high [13]. The critical VR for the vortex generation depends on the Re and channel geometry such as the ratio of channel widths of the central and sheath flows (WR). It has been predicted that the critical VR is 159 in the case of two-dimensional flow under creeping-flow conditions (Re=0; WR=1) and that it decreases with increase in the Re, in both two-dimensional and three-dimensional flow conditions (the channel height is equivalent to the channel width in the three-dimensional case) [13]. In the three-dimensional flow condition, the critical VR was predicted to be $O(10^1)$ when Re=100 [13]. We expect the vortex generated in the Newtonian fluid to be used for mixing, when multiple fluid streams flow through the central channel. However, vortex generation in Newtonian fluids can be realized only when the VR is very high according to the predictions [13], which results in the wastage of a significant amount of sheath fluid. In addition, the increase in Re will be limited by the high pressure generated in the microchannel [15].

In this work, we demonstrate that the vortex in the flow-focus-

†To whom correspondence should be addressed.
E-mail: jumin@ajou.ac.kr

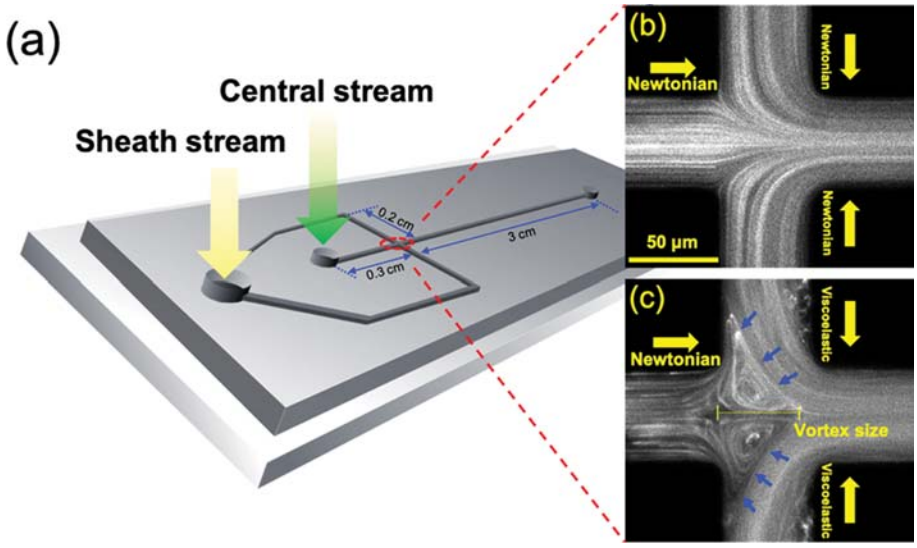

Fig. 1. (a) Schematic diagram for the flow-focusing geometry. The channel height and width are maintained at 50 mm. Representative images obtained by the flow visualization of two different cases: (b) Both the central and sheath fluids are Newtonian; (b) the central and the sheath fluids are Newtonian and viscoelastic, respectively. The Newtonian fluid is de-ionized water and the viscoelastic fluid is 100 ppm PEO aqueous solution. The yellow arrows denote the flow direction (b), (c), and the blue arrows in (c) correspond to the directions of the forces exerted by the first normal stress difference in the sheath flow. The total flow rate (Q_t and the flow rate ratio (Q_t/Q_c) are 2 ml/h and 8 (Re=4.0, Wi=6.6 and β=0.83), respectively.

ing geometry can be generated at notably lower VR values, as compared to the predicted Newtonian sheath-flow cases [13], when viscoelastic polymer solutions are used for the sheath flow. We systematically studied the effects of polymer concentration, total flow rate, and ratio of the flow rates between the sheath and central fluid streams, on the vortex generation in the flow-focusing geometry. Finally, we propose the use of viscoelastic vortex generated in flow-focusing geometry for microfluidic mixing.

EXPERIMENTAL

We used a flow-focusing microchannel to investigate the vortex generation at the junction of the central and sheath flows. The schematic diagram for the flow-focusing microchannel is presented in Fig. 1(a). The channel has two inlets and one outlet. One of the two inlets is used for the central fluid stream and the other is used for the sheath flows. The fluid stream emanating from the sheath-flow inlet is divided into two fluid streams, which meet the central fluid stream. The distance between the central stream inlet and the junction is 0.3 cm, the distance from the sharp corner to the junction in the sheath channel is 0.2 cm, and the distance from the junction to the outlet is 3 cm. The channel width (w) and height (h) are constantly 50 μm. A limited number of mixing experiments have been performed with a modified design wherein the central stream is also divided into a central and two sheath-flow streams. The microchannel is fabricated with four-walled poly(dimethyl siloxane) [PDMS], utilizing the conventional soft-lithography technique [16] (we follow the detailed processes described in the previous study [17], except that a PDMS-coated slide glass is used as the bottom layer, instead of a PDMS slab). The microchannel is pretreated to prevent the particles from sticking to the channel walls, by flowing 0.1 wt% Tween 20 (Sigma-Aldrich) aqueous solution at the flow rate of 15 μl/h for 60 min. The flow is controlled by two syringe pumps (KDS100; KD Scientific). In this work, the total flow rate (Q_t) is the sum of the flow rates of the central (Q_c) and two sheath ($2Q_s$) flow streams. The relative ratio of Q_t/Q_c, which corresponds to 1+2VR, and Q_t, are controlled to investigate the effects of the ratio of flow rates between the central and sheath streams and the total flow rate.

We used de-ionized (DI) water as the Newtonian fluid in the central stream. Dilute poly (ethylene oxide) (PEO, Mw=8,000,000 g/mol (8 M); Sigma-Aldrich) aqueous solution at three different concentrations (50, 100, 300 ppm) was prepared as the viscoelastic fluid in the sheath fluid, by dissolving the polymer in DI water. Fluorescent particles (Ex/Em=580/605 nm; F8812, Invitrogen) with 0.5 μm diameter were added at 500 ppm concentration to visualize the flow field, and 0.1 wt% Tween 20 surfactant was added to prevent the aggregation of the fluorescent particles. In the mixing experiment, 0.1 wt% red pigments (Congo red; Sigma Aldrich) and 0.1 wt% blue pigments (Evans blue; Sigma Aldrich) were added to the Newtonian fluid.

Fluorescence images for the flow-field visualization were obtained using a monochrome charged couple device (CCD) camera (DMK 23U445; ImagingSource) mounted on an inverted microscope (IX71; Olympus) with a 20× objective (N.A.=0.45). The images were taken at the rate of 30 frames per second (FPS). For the mixing experiments, a color CCD (DFK 72AUC02, ImagingSource) was used and the images were taken at 7.5 FPS. The brightness and contrast of all the images were adjusted evenly using the ImageJ (NIH) software.

The PEO concentrations ($c \leq 300$ ppm) considered in this study were in the dilute regime since the overlap concentration (c^*) is

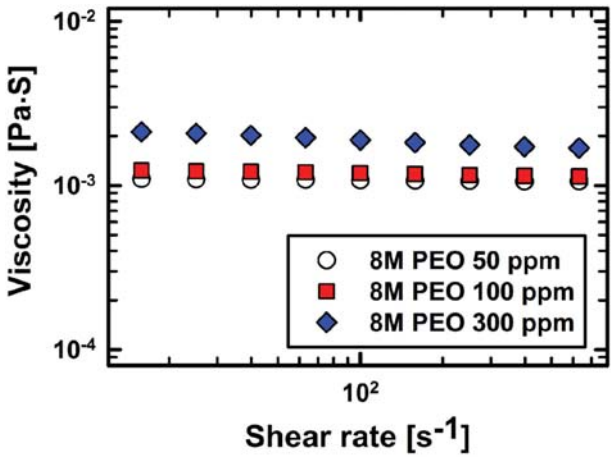

Fig. 2. Shear viscosity measurement for the 50, 100, and 300 ppm PEO [Mw=8×10⁶ (g/mol)] aqueous solutions at 20 °C using a rotational rheometer (1° cone-and-plate geometry with 60 mm diameter).

348 ppm (c^*=0.77/[μ] [18]), where [μ] denotes the intrinsic viscosity and is estimated using the relationship: [μ]=0.072$M_w^{0.65}$ (ml/g) [19]. The shear viscosities of the PEO solutions were measured with a rotational rheometer (1° cone-and-plate geometry with 60 mm diameter; AR-G2, TA Instruments) at 20 °C and a solvent trap was used to minimize the solvent evaporation during the measurement. The measured viscosities were very slightly shear-thinning for the measured shear rate range for all the polymer concentrations, as shown in Fig. 2. Therefore, we used the averaged viscosities for the measured shear-rate range: 1.1, 1.2, and 1.9 mPa·s for 50, 100, and 300 ppm PEO solutions, respectively, and the viscosity of the Newtonian fluid (DI water) was set to its standard value (1.0 mPa·s) at 20 °C. The relaxation time of the PEO solution is defined as its Zimm relaxation time (λ_Z=0.463$\frac{[\mu]M_w\mu_s}{N_A k_B T}$ [19]) and its value was estimated to be 3.4 ms, where μ_s is the solvent viscosity, N_A is Avogadro's number, k_B is the Boltzmann constant, and T is the absolute temperature.

In this study, the viscoelastic flow was analyzed using three dimensionless quantities: Reynolds (Re) and Weissenberg (Wi) numbers and the solvent contribution to the total viscosity ($\beta \equiv \mu_s/\mu_0$). Re represents the relative ratio of inertial to viscous forces, which is defined by Re=$\rho L v_s/\mu_0$, where ρ is the fluid density, L is the characteristic length scale defined by L=2hw/(h+w), and v_s is the average velocity in one sheath stream (v_s=Q_s/hw). We note that the previous definition for Re in ref. 13 is close to (2+1/VR)Re. The Weissenberg number denotes the relative ratio of elastic to viscous properties in viscoelastic flow (Wi>>1, solid-like; Wi<<1, liquid-like), and is defined by Wi=$\lambda_Z\dot{\gamma}_c$, where $\dot{\gamma}_c$ is the characteristic shear rate in the sheath flow ($\equiv v_s/(h/2)=2Q_s/h^2w$). The β values corresponding to the polymer concentrations of 50, 100, and 300 ppm are 0.91, 0.83, and 0.53, respectively.

RESULTS AND DISCUSSION

We investigated the flow dynamics in a flow-focusing microchannel, which has two inlets and one outlet. One of the two inlets is divided into two branched flows that comprise the sheath flows, and they meet the central fluid stream at the cross-slot junction, as shown in Fig. 1(a). The flow patterns at the junction are presented in Fig. 1(b); when both the central and sheath flows are Newtonian, the flow rate ratio Q_t/Q_c is 8, and the total flow rate Q_t is 2 ml/h (Re=5). The fluorescent microscopy image shows a typical convergent flow in such Newtonian sheath flow case. In contrast, when a very small amount (100 ppm) of 8M PEO was added to the Newtonian sheath fluid, the flow pattern was found to change dramatically, demonstrating a strong vortex development at the junction, as shown in Fig. 1(c). The free vortices, similar to the vortex generated by the viscoelastic sheath flow, were also predicted and experimentally observed when both central and sheath fluids were the same Newtonian fluid [13]. However, free vortices were observed only when the flow rate ratio (Q_t/Q_c) was very high (>200) at Re conditions comparable to those of the current work [13],

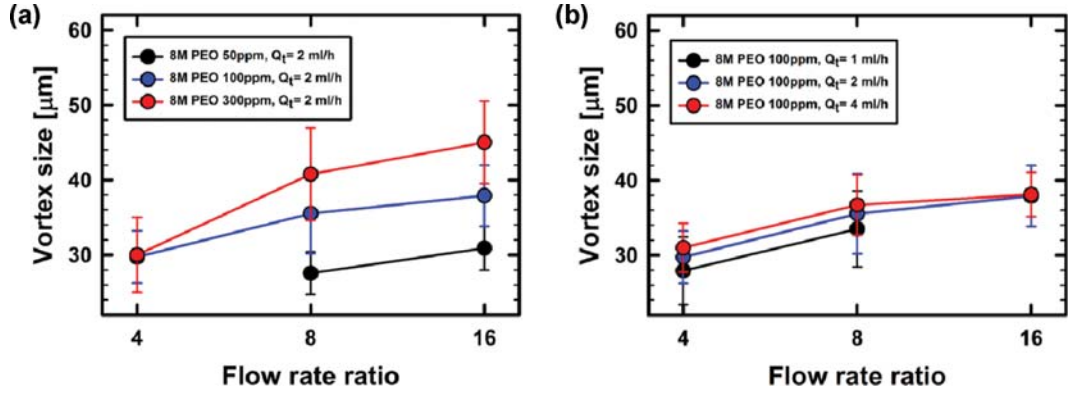

Fig. 3. (a) Vortex size according to the polymer concentration (c) and ratio of the total to central flow rates (Q_t/Q_c) at the fixed total flow rate Q_t. There is no vortex formation at c=50 ppm and Q_t/Q_c= 4. (b) Vortex size according to Q_t and Q_t/Q_c at fixed c. It is not possible to measure the vortex size, because of the unstable flow dynamics in the cross-slot region at Q_t/Q_c=16 and Q_t=1 ml/h. The data at Q_t=2 ml/h, which are presented in (a), are also included for comparison. The vortex sizes were obtained by averaging the measured values from the 20 successive images with 0.5 s interval, and the error bars denote the standard deviations of the measured values.

which is consistent with the convergent flow pattern observed in the case of the Newtonian sheath fluids at low Q_t/Q_c=8 (Fig. 1(b)). The addition of 100 ppm 8M PEO to the Newtonian solvent does not change the shear viscosity significantly (1.2 mPa·s), when compared to the solvent viscosity (1 mPa·s), as shown in Fig. 2. Therefore, we expect that the slight increase in the shear viscosity is not the origin of the vortex generation. Further, the vortex was generated at a further lower concentration (50 ppm), as shown in Fig. 3(a). Therefore, the vortex generation by the viscoelastic sheath flow, observed at the notably low flow rate ratio (Q_t/Q_c=8), can be attributed to the non-Newtonian viscoelastic effects in the PEO polymer solution. The viscoelastic properties of the dilute PEO solutions are difficult to measure with a conventional rotational rheometer when the solution viscosities are low as in the current work. The elastic properties of the PEO solutions with different molecular weights were previously characterized with capillary breakup extensional rheometer (CaBER) [19]. The current results demonstrate that the weakly elastic properties of the dilute PEO solutions can significantly change the flow dynamics in a flow-focusing microchannel.

In the viscoelastic channel flow of the polymer solution, normal stress differences are developed because of the stretching of polymer molecules, and the first and second normal stress differences (N_1 and N_2) are defined by $\tau_{ii}-\tau_{jj}$ and $\tau_{jj}-\tau_{kk}$, respectively, in the flow, where τ_{ii}, τ_{jj}, and τ_{kk} are the normal stresses in the streamwise, velocity gradient, and vorticity directions, respectively [20]. In dilute polymer solutions with constant shear viscosity, N_2 with negative sign is usually neglected owing to its much smaller magnitude when compared to that of N_1 with positive sign [21]. The viscoelastic fluid of the dilute polymer solution can be modelled with the Oldroyd-B model, which predicted the relationship of $N_1=2\lambda_Z\mu_0(1-\beta)\dot{\gamma}^2$, where $\dot{\gamma}$ corresponds to the local shear rate [17,20] and the relaxation time in dilute polymer solution is considered to be constant as λ_Z [22]. Therefore, N_1 has large values at the walls, except for the corner regions, because of the local shear rate distribution in the cross-section of a square channel, as studied previously [17]. The positive sign of N_1 predicts that the viscoelastic fluid pushes the walls in the outward direction before the viscoelastic sheath fluid enters the cross-slot junction. Then, when the viscoelastic sheath fluid meets the Newtonian central fluid at the cross-slot junction, N_1 develops inside the sheath channel, pushes the Newtonian central fluid in the backward direction of the main central stream. The backward direction is denoted by the blue arrows in Fig. 1(c). Consequently, we expected that N_1, which affects the Newtonian central stream, will eventually result in vortex formation, by the combined effects of the main flow (Q_c) and the backward-flow components generated by N_1. We postulated that the relative ratio of the backward-flow component by N_1 to Q_c is proportional to the vortex size of which the definition is presented in Fig. 1(c). We considered the horizontal length of the vortex as its size.

Next, we investigated the effects of Q_t/Q_c, c, and Q_t on the vortex size. First, we observed the change in the vortex size, according to Q_t/Q_c and c at the fixed Q_t=2 ml/h, as shown in Fig. 3(a). The vortex size increased with increasing Q_t/Q_c for all the polymer concentrations (Fig. 3(a)). The increase of Q_t/Q_c [$\equiv 1/(1-2Q_s/Q_t)$; $Q_t=Q_c+2Q_s$] indicates the increase in Q_s, and accordingly, the decrease in Q_c, at the fixed Q_t. Therefore, it is expected that the vortex size increases by the combined effects of the decrease in Q_c and the strengthening of the backward-flow component due to the N_1, in a manner proportional to $\dot{\gamma}$, as Q_t/Q_c increases and correspondingly the Weissenberg number increases. For instance, Q_c decreases from 0.5 to 0.125 ml/h and Wi increases from 11 to 14 when Q_t/Q_c changes from 4 to 16. In addition, the vortex size also increased with the increase in c (Fig. 3(a)), since N_1 is proportional to c according to the relationship of $N_1 \approx \mu_0(1-\beta)=\mu_0-\mu_s\equiv\mu_p$ [μ_p: polymer contribution to solution viscosity (μ_0); μ_p=0.1, 0.2, and 0.9 mPa·s for c=50, 100, and 300 ppm, respectively]. The vortex size consequently increases because of the strengthening of the backward-flow component by N_1 as c increases. On the other hand, we investigated the effects of the total flow rate (Q_t) on the vortex size at a fixed c=100 ppm, as shown in Fig. 3(b). Interestingly, the vortex size was not significantly sensitive to Q_t; it depended only weakly upon Q_t/Q_c ($\equiv 1+2Q_s/Q_c$) (Fig. 3(b)). Though it is not yet clear how N_1 in the viscoelastic sheath flow quantitatively determines the backward-flow component inside the cross-slot, we expected that the relative ratio of the viscous force in the central stream to the first normal stress difference in the viscoelastic sheath flow, along the boundary of the central and sheath flows, plays an important role in determining the vortex size. The relative ratio is expected to be proportional to Q_s/Q_c, based on the current experimental observations.

We also present a phase diagram for the vortex generation by the viscoelastic sheath flow in the flow-focusing microchannel, in Fig. 4, which was obtained by scrutinizing the flow dynamics in the cross-slot region for different combinations of Q_t and Q_t/Q_c at a fixed c=100 ppm. In the figure, it was not possible to generate stable flows with the current experimental setups, when Q_t/Q_c was as high as 16 and Q_t was 0.5 or 1.0 ml/h (denoted by "×"). No vortex was formed at low Q_t/Q_c or low Q_t ("N"), but the flow fields inside the cross-slot were significantly different from that of the Newtonian sheath-fluid case, which is presented in Fig. 1(b). The streamlines of the central stream (refer to the snapshot image de-

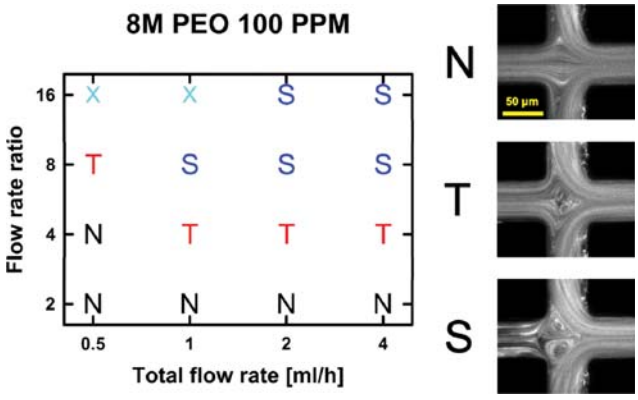

Fig. 4. Phase diagram for the vortex generation according to the total flow rate (Q_t) and flow-rate ratio (Q_t/Q_c). "×" denotes the experimental condition at which the stable flow could not be generated, and "N", "S" and "T" correspond to no vortex, stable vortex and temporarily fluctuating vortex formation, respectively.

noted by "N") were divergent in contrast to the convergent flow fields in the case of the Newtonian sheath fluid. Divergent flow fields were also observed when the Newtonian sheath fluid was used, but they were predicted with two-dimensional flow simulations under creeping conditions only when Q_t/Q_c was significantly high (≈200) [13]. A stable vortex (S), which is composed of a pair of steady vortices, was generated when both Q_t and Q_t/Q_c were high in the phase diagram, as shown in Fig. 4. In the figure, T denotes the formation of a temporarily fluctuating vortex which changes between no vortex and stable vortex states, and unstable fluctuating vortices were observed at the conditions of the boundary where no vortex was formed (N) and stable vortices occurred (S) (refer to the snapshots for each case).

Finally, we propose a novel microfluidic mixer based on the vortex generation by the viscoelastic sheath flow in the flow-focusing microchannel. The newly designed microfluidic mixer is similar to the microchannel used in the vortex-generation experiment, except that the central stream has three different streams with blue, red, and blue colors, respectively, which are generated using an additional flow-focusing geometry, as shown in Fig. 4(a) and 4(b). The total flow rate of the red-dyed stream is controlled to be the same as the flow rate of the blue-dyed streams utilizing a syringe pump (KDS 210; KD Scientific) having two equivalent syringes. The central stream with three sub-streams meets the sheath flow at the cross-slot region, denoted by a rectangle in Fig. 4(a). We investigated how the viscoelastic sheath flow affected the mixing of the central stream, as shown in Fig. 4(b) (Q_t=2 ml/h; Q_t/Q_c=8), where 300 ppm 8M PEO solution was used as a viscoelastic sheath fluid. The blue-dyed streams were clearly discernible from the red stream in the cross-slot region when the sheath fluid was Newtonian, while those streams were significantly mixed in the case of the viscoelastic sheath flow, as shown in Fig. 4(b). The current experimental data suggest that vortex generation by viscoelastic sheath flow can enhance mixing in microchannels. The microchannel used in this work can be fabricated using the standard single-layer soft-lithography technique, which is in contrast to the herringbone-type channel [7]. Therefore, there will be no additional process for channel fabrication. In addition, the polymer used in this work is commercially available and the mixing is expected to be enhanced by simply adding a small amount of polymer to the sheath fluid.

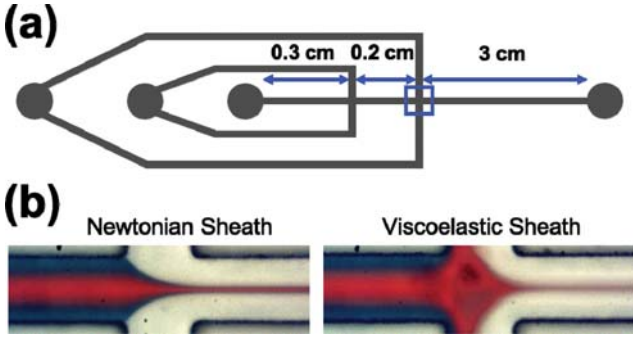

Fig. 5. (a) Schematic diagram for novel microfluidic mixer based on the vortex generation by the viscoelastic sheath flow in a flow-focusing microchannel. (b) Snapshots of the mixing experiments when the sheath fluid is Newtonian or viscoelastic (Q_t/Q_c=8 and Q_t=2 ml/h).

CONCLUSIONS

We investigated vortex generation in a microfluidic flow-focusing geometry, especially when the sheath fluid is a viscoelastic polymer solution. The current experimental results demonstrated that the vortex was generated at a much lower ratio of total flow rate to the central flow rate when the sheath fluid was viscoelastic as compared with Newtonian sheath flow cases. The current experimental finding is a novel viscoelastic flow phenomenon, and we elucidated that the vortex was generated by the combined effects of the central main-stream and the backward-flow component induced by the first normal stress difference developed in the viscoelastic sheath flow. We demonstrated that the vortex size is affected significantly by the relative ratio of the total flow rate to the central flow rate and the polymer concentration; however, it is not very sensitive to the total flow rate. These observations suggest that the relative ratio of the central main-stream and the backward-flow component induced by the first normal stress difference is expected to be proportional to that of the central to the sheath flow rates, which demands further studies. We also demonstrated that vortex generation can be engineered to enhance the mixing in the flow-focusing geometry, which will contribute to the development of micromixers.

ACKNOWLEDGEMENT

This research was supported by the Research Program through the National Research Foundation of Korea (NRF) (Nos. NRF-2016R1A2B4012328 and NRF-2018R1A5A1024127).

REFERENCES

1. E. K. Sackmann, A. L. Fulton and D. J. Beebe, *Nature*, **507**, 181 (2014).
2. Y. Liu and X. Jiang, *Lab Chip*, **17**, 3960 (2017).
3. D. Dendukuri, D. C. Pregibon, J. Collins, T. A. Hatton and P. S. Doyle, *Nat. Mater.*, **5**, 365 (2006).
4. P. Tabeling, *Introduction to microfluidics*, Oxford University Press, New York (2006).
5. C.-Y. Lee, C.-L. Chang, Y.-N. Wang and L.-M. Fu, *Int. J. Mol. Sci.*, **12**, 3263 (2011).
6. R. H. Liu, M. A. Stremler, K. V. Sharp, M. G. Olsen, J. G. Santiago, R. J. Adrian, H. Aref and D. J. Beebe, *J. Microelectromech. S.*, **9**, 190 (2000).
7. A. D. Stroock, S. K. W. Dertinger, A. Ajdari, I. Mezić, H. A. Stone and G. M. Whitesides, *Science*, **295**, 647 (2002).
8. T. Burghelea, E. Segre, I. Bar-Joseph, A. Groisman and V. Steinberg, *Phys. Rev. E*, **69**, 066305 (2004).
9. A. Groisman and V. Steinberg, *Nature*, **405**, 53 (2000).
10. A. Groisman and V. Steinberg, *Nature*, **410**, 905 (2001).
11. L. E. Rodd, T. P. Scott, D. V. Boger, J. J. Cooper-White and G. H. McKinley, *J. Non-Newt. Fluid Mech.*, **129**, 1 (2005).
12. S. O. Hong, J. Cooper-White and J. M. Kim, *Appl. Phys. Lett.*, **108**, 014103 (2016).

13. M. S. N. Oliveira, F. T. Pinho and M. A. Alves, *J. Fluid Mech.*, **711**, 171 (2012).
14. S. P. Sullivan, B. S. Akpa, S. M. Matthews, A. C. Fisher, L. F. Gladden and M. L. Johns, *Sensor Actuat. B Chem.*, **123**, 1142 (2007).
15. J. B. You, K. Kang, T. T. Tran, H. Park, W. R. Hwang, J. M. Kim and S. G. Im, *Lab Chip*, **15**, 1727 (2015).
16. Y. Xia and G. M. Whitesides, *Angew. Chem. Int. Ed.*, **37**, 550 (1998).
17. S. Yang, J. Y. Kim, S. J. Lee, S. S. Lee and J. M. Kim, *Lab Chip*, **11**, 266 (2011).
18. W. W. Graessley, *Polymer*, **21**, 258 (1980).
19. V. Tirtaatmadja, G. H. McKinley and J. J. Cooper-White, *Phys. Fluids*, **18**, 043101(2006).
20. R. B. Bird, R. C. Armstrong and O. Hassager, *Dynamics of polymeric liquids*, Wiley Interscience, New York (1987).
21. J. J. Magda, J. Lou, S. G. Baek and K. L. DeVries, *Polymer*, **32**, 2000 (1991).
22. Y. G. Liu, Y. G. Jun and V. Steinberg, *J. Rheol.*, **53**, 1069 (2009).